RESEARCH ARTICLE

How to cite: G.Naga Chandrika, J. Karpagam, Titus Richard, Finney Daniel Shadrach and T. Triwiyanto, QCML: Qualified Contrastive Machine Learning methodology for infectious disease diagnosis in CT images, Journal of Electronics, Electromedical Engineering, and Medical Informatics, vol. 6, no. 2, pp. 195-205, April 2024.

QCML: Qualified Contrastive Machine Learning methodology for infectious disease diagnosis in CT images

G.Naga Chandrika[1] , J. Karpagam[2] , Titus Richard[3] , Finney Daniel Shadrach[4] , and T. Triwiyanto[5]

[1] Department of Information Technology, VNR VJIET, Hyderabad, 500090 Telangana, India
[2] Department of Electrical and Electronics Engineering, Karpagam Academy of Higher Education University, Coimbatore, India
[3] Department of Biosciences, Saveetha School of Engineering, Saveetha Institute of Medical and Technical Sciences, Saveetha University, Chennai, India
[4] Department of ECE, KPR Institute of Engineering and Technology, Coimbatore, India.
[5] Department of Medical Electronics Technology, Poltekkes Kemenkes Surabaya, Surabaya, Indonesia
Corresponding author: Titus Richard (e-mail: titusrichad@gmail.com)

ABSTRACT The COVID-19 pandemic has had a terrible effect on human health, and computer-aided diagnostic (CAD) systems for chest computed tomography have emerged as a potential alternative for COVID-19 diagnosis. Yet, since the cost of data annotation may be excessively costly in the medical area, there is a shortage of data that has been annotated. A considerable quantity of labelled data is required in order to train a CAD system to a high level of accuracy. The study aims to describe an automatic and precise COVID-19 diagnostic method that utilizes a restricted amount of labelled CT images to solve this problem. The framework of the system is known as Qualified Contrastive Machine Learning (QCML), and the improvements that we have made may be summed up as follows: 1) In order to make use of all of the image's characteristics, we combine features with a two-dimensional discrete wavelet transform. 2) We employ the COVID-Net encoder with a redesign that focuses on the efficiency of learning and the task specificity of the data. 3) In order to strengthen our capacity to generalize, we have implemented a novel pertaining technique that is based on Qualified Contrastive Machine Learning. 4) In order to get better categorization results, we have included an extra auxiliary work. The application of Qualified Contrastive Machine Learning methodology for infectious disease diagnosis in CT images offers an accuracy of 93.55%, a recall of 91.59%, a precision of 96.92%, and an F1-score of 94.18%, demonstrating the potential for accurate and efficient COVID-19 diagnosis with limited labelled data.

INDEX TERMS Machine Learning (ML), COVID-19 Diagnosis, Discrete Wavelet Transform (DWT), Computed Tomography (CT) Images, Classification.

I. INTRODUCTION

Coronavirus (Covid-19), which initially appeared in Wuhan, China in December 2019, and is swiftly becoming a worldwide pandemic [1] is caused by the severe acute respiratory syndrome coronavirus 2 (SARS-COV-2), which is responsible for producing severe acute respiratory syndrome. More than 410 million cases have been documented up to this point, and about 6 million fatalities have been attributed to the disease, as stated by the World Health Organization (WHO) [2]. Because of the rising number of fatalities and cases, the World Health Organization (WHO) designated the coronavirus illness as a Covid-19 pandemic in March of 2020. This caused a number of nations to shut down their borders and institute curfews as preventative measures [3]. Covid-19 predominantly affects the respiratory system, such as the

lungs, and often produces symptoms that are comparable to those of pneumonia [4]. Fever, coughing, sneezing, and shortness of breath are among of the most common symptoms, and the disease is very infectious because it spreads by respiratory droplets, such as when an infected person coughs or sneezes. The elderly and those who suffer from ongoing medical conditions are at a greater risk of contracting the Covid-19 infection.

In addition to RT-PCR testing, imaging techniques such as computed tomography (CT) and chest X-ray (X-ray) are used for the purpose of identifying the virus known as Covid-19, which mostly affects the lungs [5]. Patients with pneumonia caused by Covid-19 may be accurately diagnosed with the use of CT imaging to identify characteristic radiographic findings. Yet, in order to properly analyse these photos, specialised

Journal of Electronics, Electromedical Engineering, and Medical Informatics
Multidisciplinary: Rapid Review: Open Access Journal
Vol. 6, No. 2, April 2024, pp: 195-205; eISSN: 2656-8632

medical doctors are necessary. CT and X-ray imaging both offer certain benefits in early detection in comparison to RT-PCR assays, but both methods also have some limitations. Artificial intelligence (AI) and deep learning (DL) techniques are being investigated as a potential alternative to help in the early diagnosis of Covid-19 and to expedite the treatment process. This will be accomplished by enabling medical professionals to quickly and accurately diagnose the disease utilising CT and X-ray images [13-15]. Researchers make extensive use of artificial intelligence and deep learning approaches for the identification of Covid-19 infection using X-ray and CT images. In comparison to more conventional approaches, the adoption of deep learning techniques has increased significantly because of their superior efficiency [16]. Deep learning architectures, in contrast to machine learning and conventional approaches, do not need the extraction of features from the data during the pre-processing step. This is one of the most significant factors that drove academics to focus their attention on this area of study.

Deep hybrid learning (DHL) and deep boosted hybrid learning (DBHL) are the names of two novel deep learning-based models that were suggested for successful detection of Covid-19 in X-ray datasets in another work that was conducted by [17]. According to the findings of this research, which makes use of X-ray pictures of two different classes (Covid and Non-Covid), the method has an accuracy of 98.53%. According to the findings of this research, doing performance evaluations using just binary class X-ray pictures is detrimental to the overall performance of the designs being investigated. So it is essential to make use of a variety of data sets while attempting to discover Covid-19 [18]. The number of classes and the kind of image both have a role in the degree to which a CNN architecture is successful.

Our strategy takes use of data obtained from a variety of sources and overcomes the problem of a lack of large-scale labelled data by using these data. To be more specific, we employ the recently specifically created COVID-Net [19] for experimental research. The architecture of this network has been redesigned to better accommodate the needs of our project. In addition, while we are working on the downstream job of the system that we have suggested, we have included a cooperative learning method that utilises a contrastive learning object [20]. An approach like this one not only boosts speed, but it also gathers semantic representations that are very close to one another yet have hazy borders inside a category domain like this one. In order to stabilise the pipeline and capture additional characteristics in advance of training, the DWT technique will be deployed. Using a publicly available COVID-19 CT dataset, we conduct in-depth experiments to test and assess our methodology for COVID-19 identification tasks [21]. According to the findings, our method is successful in obtaining substantial CT feature representations, which allows appropriate classifications to be made between COVID-19 patients and normal patients using the annotated data source. The research gap in this context is the requirement for an automated and accurate technique for diagnosing COVID-19 using a small number of annotated CT scans and a large number of unlabeled CT images. Existing approaches

might struggle due to a lack of labelled data, limiting their ability to properly diagnose the condition. The suggested method addresses this gap by combining QCML and discrete wavelet transform to increase the accuracy and efficiency of COVID-19 detection. The most important findings and contributions of this research are presented in the following points,

1. To address the issue of inadequate labelled data, an automated and precise method for diagnosing COVID-19 based on a small number of labelled CT scans and a large number of unlabeled CT images is required.

2. In order to make the most of all of the characteristics included inside the pictures, we combine QCML with discrete wavelet transform.

3. The process involves extracting both spectral and temporal features from a CNN that has been trained using heatmaps derived from a multilevel discrete wavelet transform (DWT). These spectral-temporal features are then combined with spatial features that are extracted from another CNN that was trained using the original multiview CT images. This integration of spectral-temporal and spatial features is intended to improve the accuracy and effectiveness of the overall classification or analysis task.

The paper is structured as follows: In Section 2, the methods, datasets, and proposed pipeline are described in detail. This section provides a comprehensive overview of the approach taken by the authors in their research. Section 3 outlines the experimental setup, including the parameters that were adjusted for the CNNs and the metrics that were used for evaluation. This section provides a clear understanding of the experimental design and the specific factors that were considered in the study. The results are presented in Section 4, which highlights the key findings of the research. This section provides a detailed analysis of the performance of the proposed method, including any limitations or challenges that were encountered. Section 5 discusses the results in more detail, providing a critical analysis of the findings and their implications. This section also highlights the contributions of the research and its potential future applications. Finally, Section 6 concludes the paper by summarizing the main findings, highlighting the significance of the research, and providing recommendations for future work.

II. PROPOSED MODEL

Convolutional Neural Networks, also known as CNNs, are powerful models that can achieve high levels of accuracy when classifying data in multi-class problems. One of the main advantages of CNNs is their ability to learn and improve their classification performance over time without human intervention. The architecture of a CNN is based on a coordinated arrangement of multilayer perceptrons, where each neuron in one layer is connected to all the neurons in the next layer. This highly interconnected structure allows CNNs to extract and identify features from input data with remarkable accuracy. Sample Image Dataset is shown in FIGURE 1. DataSet contains 6432 x-ray images for training and 1286 images for testing. Chest X-ray images are typically

Journal of Electronics, Electromedical Engineering, and Medical Informatics
Multidisciplinary: Rapid Review: Open Access Journal

Vol. 6, No. 2, April 2024, pp: 195-205; eISSN: 2656-8632

2D and can vary in resolution, but a common size is around 1024x1024 pixels.
https://www.kaggle.com/datasets/prashant268/chest-xray-covid19-pneumonia.

The building blocks of a CNN are the convolutional layer and the rectified linear unit (ReLu). The convolutional layer is the most important component of a CNN, responsible for extracting key features from the input data. The ReLu is an activation function that helps to increase the non-linearity of the CNN, allowing it to better represent complex relationships between features. Overall, the architecture and design of CNNs enable them to perform exceptionally well in complex classification tasks, making them a popular choice for image recognition, natural language processing, and other AI applications.
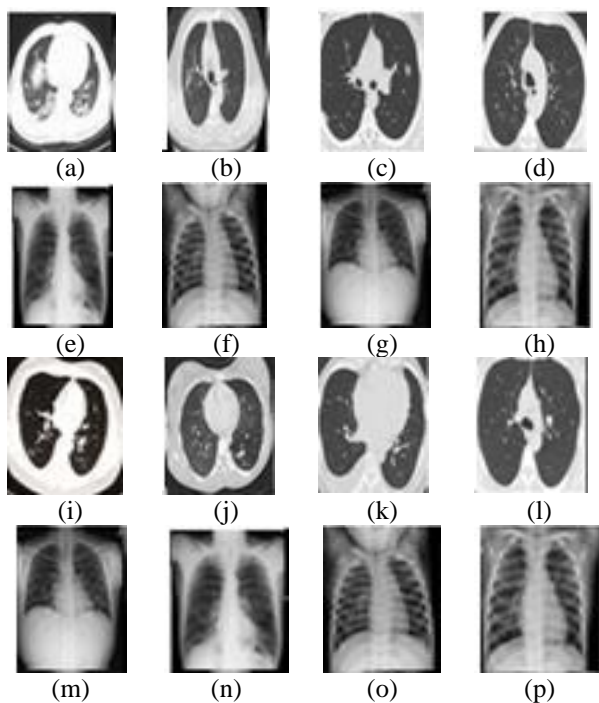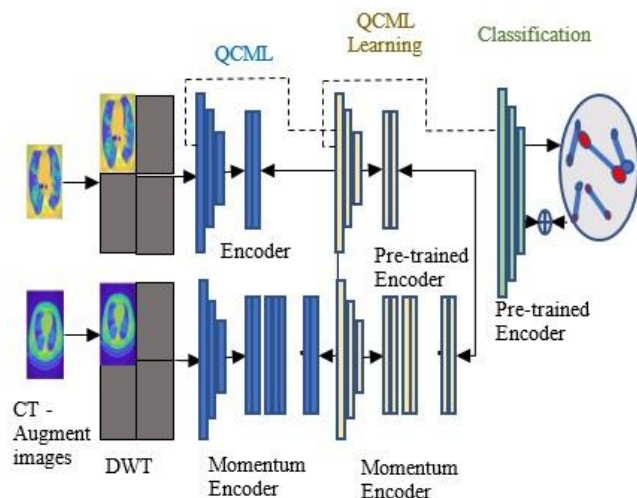

FIGURE 1. Sample dataset images

FIGURE 2. Proposed Model

The input data is processed by convolving it with nuclei using convolution filters that span across the entire visual field. As a result, the convolutional operation enables the extraction of both simple, small patterns and more complex, detailed patterns from the input data. This hierarchical network structure allows for the extraction of the most important feature maps, improves the generalization capability of the model, and reduces the computational complexity required for training and inference [22]. The convolution operation is a fundamental mathematical operation that underlies this process, and it can be expressed mathematically as [23]. The proposed model is shown in FIGURE 2.

A. WAVELET DECOMPOSITION

It is possible to localize a signal in both the time domain and the frequency domain using the wavelet transform as shown in FIGURE 3 and FIGURE 4, which makes it a helpful tool for signal classification. This feature sets the wavelet transform apart from other techniques of transformation. Wavelet is used for analysing CT scans for the primary reason that it can efficiently detect obscure or hidden characteristics within the pictures. This is the major reason why wavelet is selected. By scaling and shifting a mother wavelet that already exists, it is possible to generate a wavelet of a higher order as shown in Eq. (1) and Eq. (2) [24].

$$W_\emptyset[j_0, k] = \frac{1}{\sqrt{M}}\sum_n x[n]\emptyset_{j_0,k}[n] \qquad (1)$$

$$W_\psi[j, k] = \frac{1}{\sqrt{M}}\sum_n x[n]\psi_{j,k}[n], \ for j \geq j_0 \qquad (2)$$

where, $W\_\emptyset [j\_0,k]$ and $W\_\psi [j,k]$ are the approximation coefficients and detail coefficients, respectively, and the inverse DWT is given by Eq. (3) [25]. Table I represents various deep learning models used for Classification

$$x[n] = \frac{1}{\sqrt{M}}\sum_n x[n]\emptyset_{j_0,k}[n] + \frac{1}{\sqrt{M}}\sum_n x[n]\psi_{j,k}[n], \ for j \geq j_0 \quad (3)$$
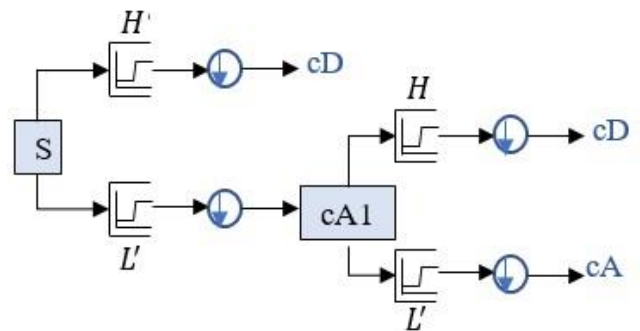

FIGURE 3. Wavelet Decomposition

A higher-order wavelet is derived from a fixed mother wavelet by applying scaling and shifting operations. Let's assume (x) represents a continuous function with square integrability. In the context of a real-valued wavelet (x), we define the continuous wavelet transform of (x) using Eq. (4) and (5) [26]. These equations capture the mathematical representation of the transformation process, where the wavelet is scaled and shifted to analyse different components of the input function (x).

$$T_\psi(j, k) = \int_{-\infty}^{+\infty} f(x)\psi_{j,k}(x).dx \qquad (4)$$

Journal of Electronics, Electromedical Engineering, and Medical Informatics
Multidisciplinary: Rapid Review: Open Access Journal

Vol. 6, No. 2, April 2024, pp: 195-205; eISSN: 2656-8632

$$\psi_{j,k}(x) = \frac{1}{\sqrt{2^j}}\psi\left(\frac{x-2^j k}{2^j}\right); \quad (j,k) \in \mathbb{Z}^2 \tag{5}$$

TABLE 1
Various Deep Learning models used for classification

Model	Input size	Learning rate	Opti-mizer	Software	Batch size
Dense_Net	224 × 224	0.0001	Adam	TensorFlow, Keras	64
Alex_Net	224 × 224	0.0001	Adam	TensorFlow, Keras	64
Res_Net	224 × 224	0.0001	Adam	TensorFlow, Keras	64
CspNet	224 × 224	0.0001	Adam	TensorFlow, Keras	64
VGG16	128 × 128	0.0001	Adam	TensorFlow, Keras	64
VGG19	128 × 128	0.001	Adam	TensorFlow, Keras	64
CovXNet	224 × 224	0.0001	Adam	TensorFlow, Keras	64
DarkCovidNet	256 × 256	0.003	Adam	TensorFlow, Keras	64
Proposed	128 × 128	0.0001	Adam	TensorFlow, Keras	64

The parameters of j and k are the wavelet scale and translation factors, respectively. Orthogonal wavelets Eq. (6) validated by 2^j carry signal variations at the resolution 2^{-j} [27].
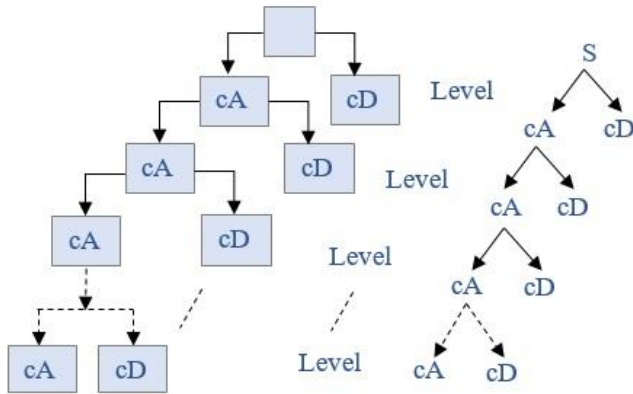

FIGURE 4. High and Low Frequency decomposition

$$DWT_{f(n)} = \begin{cases} s_{j,k} = \sum_n f(n) l_{n-2^j k,} \\ d_{j,k} = \sum_n f(n) h_{n-2^j k,} \end{cases} \tag{6}$$

where $s_{j,k}$ refers to the low-frequency component and $d_{j,k}$ refers to the high-frequency component. we can deduce the IDWT Eq. (7) process to reconstruct s from $s_{j,k}$ and $d_{j,k}$ [28].

$$s_n = \sum_k (l_{n-2^j k} s_{j,k} + h_{n-2^j k} d_{j,k}) \tag{7}$$

B. ENCODERS
A traditional encoder is designed to be versatile and compatible with various types of network architectures, allowing it to be applied to different types of tasks. However, the differences between different encoders can vary significantly, ranging from substantial variations to minor variances. In our specific research, we chose to utilize COVID-Net, a popular and well-known encoder, as our

chosen encoders fk and fq. These encoders were trained to learn representations based on lung CT images for the purpose of COVID-19 detection. This architectural choice allows for effective representation learning while controlling the computational complexity. The architectural advantages of COVID-Net, particularly its lightweight residual layers, align well with the internal structure of our QCML method. This alignment contributes to the successful integration of COVID-Net as the encoder in our research framework as shown in FIGURE 5. COVID-Net was first designed for the purpose of categorising CXR pictures; nevertheless, it has the potential to be beneficial for improving pattern recognition due to the fact that CT scans include more exact features than CXR images do. On the other hand, if there isn't any adequate coordination, this variation might result in greater computational load and a reduction in output accuracy. In order to solve this problem, we have included batch normalisation (BN) into the COVID-Net architecture. This will help minimise the amount of internal covariate shift (ICS) [24] and increase representation learning stability while the network is being trained. After the input photos and at each central hub in the top sector of the architecture, BN layers have been purposefully created. This is due to the fact that the bottom sector is filled to the brim with convolution layers, and the addition more BN layers would lead to a considerable rise in the number of parameters as well as the complexity of the calculation.

We choose a neuron x_k at random from a layer to guarantee that the amount of processing that is used is as efficient as possible. The BN operation may be stated mathematically as represented in Eq. (8) [29].

$$y_k = \gamma_k \hat{y}_k + \beta_k, \quad where \; \hat{y}_k = \frac{x_k - E(x_k)}{\sqrt{Var(x_k)}} \tag{8}$$

E(.) and Var(.) denote the average and variation of the input neurons, respectively. On the other hand, γ and β are trained parameters from layers that are utilized to revert the transformation of the activation and make the network more flexible.
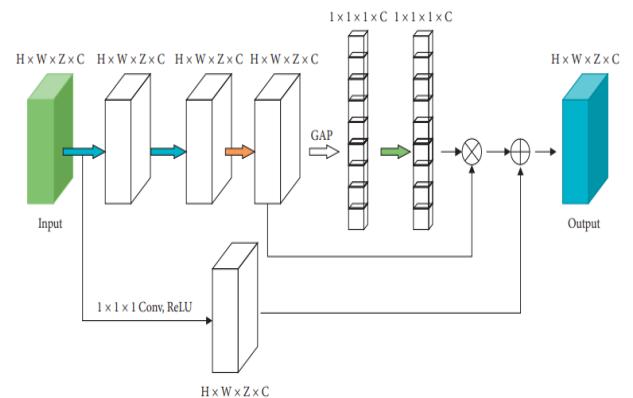

FIGURE 5. Network structure of the feature encoding block.

C. QUALIFIED CONTRASTIVE MACHINE LEARNING (QCML)
In recent years, contrastive machine learning has been an increasingly prominent study subject, particularly when applied to the processing of medical images. This trend is

especially evident in the context of the medical field. Extracting meaningful representations from unlabelled information by using a variety of pretext tasks, such as mask image modelling and contrastive machine learning, is the goal of this methodology, which is based on deep learning networks. The auxiliary work is finished off by designing a loss function, which also serves to fine-tune the features that will be used in the subsequent tasks, such as semantic segmentation, object identification, and picture classification [25]. We have decided to use a contrastive task as the contrastive machine learning pretext task for the COVID-19 diagnostic downstream task. This choice was made in order to maximise accuracy. Contrastive machine learning is one of the most successful ways of contrastive machine learning because it permits the learning of excellent representations without the need for annotated datasets. This makes it one of the most effective methods of contrastive machine learning. In this method, several unlabelled photographs are compared to one another, and the contrastive loss is determined by analysing the degree to which the images are alike and differently from one another [26]. After the pre-training phase, which took place at the QCML stage, the encoder was moved into the classification stage in preparation for the COVID-19 detection in input images. In contrast to the contrastive loss that we imposed during the contrastive machine learning, we will now add a similarity function in the following manner as shown in Eq. (9) [30].

$$sim(u, v) = \frac{u^T v}{\|u\|_2 . \|v\|_2} \tag{9}$$

The notation (u, v) refers to a pair of embedding characteristics that were taken from the classifier's average pooling layer. For the sake of dimensionality reduction, we make the decision to implement an extra projection micro network Z(.). As a result of handling things in this manner, the dimension of the embedding's is brought down to 128, and the similarity function is modified to read as Eq. (10) [31].

$$sim(u, v) = \frac{Z(u).Z(v)}{\|Z(u)\|_2 . \|Z(v)\|_2} \tag{10}$$

Contrary to the QCML stage, the contrastive loss that is used for the auxiliary work is planned in the following manner as shown in Eq. (11) [31].

$$l = -log \frac{\exp(sim(u,v)/\tau)}{\sum_{k=1}^{k} I.\exp(sim(u,v)/\tau)} \tag{11}$$

where I is intended to function as an indicator and may take on the value 0 or 1 depending on whether or not (u, v) is positive or negative. Each batch of data will be entered into a calculation that will simultaneously determine the cross-entropy loss and the contrastive loss. By using our strategy, it is possible to improve the performance of the model in a manner that is invariant to the domain, which in turn improves the performance of the bi-classification.

Algorithm:

1. Let the batch size N_s & N_c, Dataset I D_1, Dataset D_2, Temperature τ, f_q, f_k, wavelet filter T_f, g, augmentation function T, dictionary q and the projection head z be the input.

2. **Initialize** the encoder f pretrained on LUNA dataset for query and keys.
$$f_q - f_k = f$$

3. **Create** the convolutional neural network and Resnet
 Create the threshold Image
  for i=1: row length of N_s & N_c
  *f*or i=1: column length of N_s & N_c
  if N_s & $N_c(x,y)$<254
  N_s & N_c (x,y)=0
  else
   N_s & N_c (x,y)=1
  end if
  end for

4. For **sampling from D_1**, perform the following steps for mini- batch$(xi)_{i=1}^{Ns}$.
 for i ∈ {1,....,N_s} do
  Select augmentation functions t, t' from T:
  $X_{2i-1} = t(x_i)$, $\hat{x}_{2i-1} = t'(x_i)$:
  Transform augmented images with T_f:
  $X_{2i-1} = T_f(x_{2i-1})$, $\hat{X}_{2i-1} = T_f(\hat{X}_{2i-1})$;
  $h_{2i-1} = f_k(x_{2i-1})$, $h_{2i} = f_q(\hat{X}_{2i-1})$;
  $z_{2i-1} = g(h_{2i-1})$, $z_{2i} = g(h_{2i})$;
  $l_{pos} = \{z2i-1.z2i\}_{i=1}^{Ns}$, $I_{neg} = \{z2i-1.q\}_{i=1}^{Ns}$;
  end for
  l = concate ([l_{pos}, l_{neg}], dim = 1);
  Î = zeros_like(x_i);
  l_{con} = CrossEntropyLoss(l/τ,Î);
  Update f_k to minimize l_{con};
  Update f_q via $sim(u,v) = \frac{u^T v}{\|u\|_2 . \|v\|_2}$
  Enqueue (q, z_{2i-1});
  Dequeue (q);
 end for
 return f_k;

5. For **sampling from D_2**, perform the following steps for mini- batch$(xi, yi)_{i=1}^{Nc}$.
  f = f_k;
  Transform input images with T_f;
  $X_i = T_f(x_i)$;
  $\hat{h}_i = f(X_i)$;
  $\hat{z} = Z(\hat{h}_i)$;
  $\hat{y}_i$ = classifier($\hat{h}_i$);
  l_{ce} = CrossEntropyLoss($\hat{y}_i$, y_i);
  Calculate contrastive loss via $L(\hat{y}, y) = -\sum y_i \log(\hat{y}_i)$;
  l_{con} = NTXentLoss($\hat{z}$,y_i);
  $l_{overall} = l_{ce} + l_{con}$;
  Finetune f to minimize $l_{overall}$;

 end for

6. **Compute** accuracy, precision, recall, AUC.
 a. Accuracy = ((TP+TN)/(TP+TN+FP+FN))* 100
 b. Sensitivity = (TP/TP+FN) * 100
 c. Specificity = (TN/TN+FP) * 100
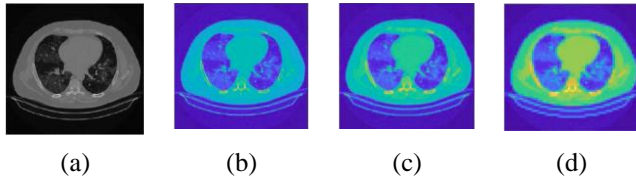
7.   **Return** accuracy, precision, recall, AUC.

<div align="center">(a)   (b)   (c)   (d)</div>

<div align="center">**FIGURE 6.** Network structure of the feature encoding block.</div>

<div align="center">(a)   (b)   (c)   (d)</div>
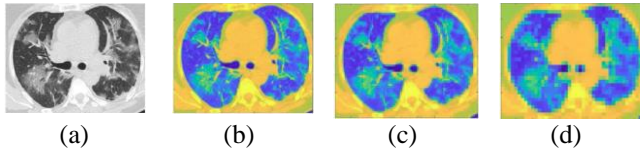
<div align="center">**FIGURE 7.** Heatmap of various levels of DWT for Dataset II</div>

The various datasets heat maps are shown in FIGURE 6 and FIGURE 7.

III.   TRAINING AND OPTIMIZATION OF THE PROPOSED ARCHITECTURE

The architecture that has been proposed is subjected to a training process facilitated by a backpropagation algorithm. This algorithm is responsible for adjusting the network's weights and biases to optimize its performance. In the case of training multi-class datasets, the chosen cost function is Cross-Entropy Eq. (12). This particular cost function is designed to measure the dissimilarity between the predicted output probabilities and the true labels of the multi-class dataset. It takes into account the logarithm of the predicted probabilities, ensuring that the model is penalized for incorrect predictions and encouraged to make more accurate ones.   On the other hand, when dealing with two-class datasets, the binary cross-entropy Eq. (13) is employed as the cost function. This specific cost function is tailored to the nature of binary classification tasks. It evaluates the discrepancy between the predicted probabilities and the true binary labels, aiming to minimize the divergence between them. By calculating the logarithm of the predicted probabilities, it effectively captures the errors made by the model and guides the learning process towards achieving better classification performance [23].

$$L(\hat{y}, y) = -\sum y_i \log (\hat{y}_i) \tag{12}$$
$$L_{BCE} = -\frac{1}{n}\sum((y_i \log (\hat{y}_i)) + (1 - y_i).\log (1 - \hat{y}_i)) \tag{13}$$

In the given context, the variable "n" represents the total number of samples within the dataset. The variable "y" denotes the true or actual value associated with each sample, while "y-hat" ($\hat{y}$) represents the predicted value for the corresponding sample.   To update the weights within the architecture during the training process, the Adam optimization algorithm is utilized. This algorithm, referenced as "Adam optimization [27]," is a popular choice for optimizing neural network models. It combines the advantages of both adaptive gradient descent (AdaGrad) and root mean

square propagation (RMSprop) algorithms. During the optimization process, the Adam algorithm employs a learning coefficient, denoted as η (eta), which determines the step size or rate at which the weights are updated [28, 29]. The learning coefficient η can vary at different time steps during the training process, denoted as t. The specific value of η at a given time step t is determined by the Adam optimization algorithm as represented an Eq. (14) – Eq. (16) [24].

$$w_{t+1}^j = w_t^j - \eta \frac{V_t}{\sqrt{S_t + \varepsilon}} - \times g_t \tag{14}$$

$$V_t = \beta_1 \times V_{t-1} - (1 - \beta_1) \times g_t \tag{15}$$

$$S_t = \beta_2 \times S_{t-1} - (1 - \beta_2) \times g_t^2 \tag{16}$$

In the provided explanation, the variable "w" represents the weights within the architecture. The hyperparameters β_1 and β_2 correspond to specific coefficients used in the Adam optimization algorithm. The coefficient η denotes the learning rate, which determines the step size for weight updates during training, with its value varying at different time steps denoted as t. The gradient at time step t is represented by g_t. Furthermore, V_t and S_t symbolize the exponential moving averages of the gradients and the squares of gradients, respectively, along with the weights w_t. Within the proposed architecture, the rectified linear unit (ReLU) activation function is employed after each convolution operation. This activation function is described mathematically in Eq. (17) referenced as [30,31]. The ReLU activation function is widely used in neural networks and is defined as follows:

$$f(x)_{Relu} = \max \{0, x\} \tag{17}$$

Fully connected layers (FC) are integral components of convolutional neural network (CNN) architectures. In FC layers, every neuron in the preceding layer is connected to every neuron in the subsequent layer. These connections enable the calculation of the degree to which each value aligns with a particular class or category. In the architecture's final layer, the output of the FC layer is combined with activation functions such as sigmoid, support vector machine (SVM), softmax, and others to facilitate the prediction of classes. In the specific study mentioned, the softmax activation function is utilized for classification purposes. The softmax activation function computes a probability distribution for a given set of output categories. This distribution assigns probabilities to each category based on the input values. Eq. (18) referenced as [23] presents the mathematical representation of the softmax activation function used in this study.

$$Z^k = \frac{e^{x^k}}{\sum_{i=1}^n e^{x^k}} \tag{18}$$

In the given context, x represents the input vector to the softmax activation function. The variable n corresponds to the number of classes or categories in the classification task. The index k ranges from 1 to n indicating each individual class. The output vector of the softmax activation function is denoted as Z. It consists of n elements, with each element representing

the probability or likelihood of the input belonging to the corresponding class k. One of the key properties of the softmax function is that the sum of all the elements in the output vector Z is equal to 1. This property ensures that the output vector represents a valid probability distribution over the classes, as probabilities must sum up to 1.

IV. RESULTS

Typically, studies that involve only two classes tend to have higher success rates compared to studies involving multiple classes. In comparison, the proposed architecture gave a rate of 99.85% accuracy. Nevertheless, the success rates of these approaches are contingent on the datasets that were used by the researchers. This includes the quantity of samples and classes that were included within the datasets, both of which might have an effect on the effectiveness of the designs. Eq. (19), Eq. (20), and Eq. (21) explain how classification algorithms are assessed based on accuracy, sensitivity, and specificity [24,25]. Table II lists the model's attainment values. FIGURE 5 shows how the number of epochs affects accuracy.

$$Accuracy = ((TP+TN)/(TP+TN+FP+FN))* 100 \quad (19)$$
$$Sensitivity = (TP/TP+FN) * 100 \quad (20)$$
$$Specificity = (TN/TN+FP) * 100 \quad (21)$$

TABLE 2
Performance comparison with dataset i

| Model	Acc. (%)	Prec.	Recall	F1-Score	Spec. (%)	AUC (%)
DenseNet	96.06	96.68	95.53	96.43	97.55	97.22
AlexNet	92.83	92.23	92.3	93.18	93.1	93.97
ResNet	94.65	94.08	94.12	95.03	94.95	95.82
CspNet [21]	93.84	93.25	93.31	94.2	94.12	94.99
VGG16	49.2	48.11	48.67	49.06	48.98	49.85
VGG19	49.2	48.11	48.67	49.06	48.98	49.85
CovXNet [22]	96.87	96.29	96.34	97.24	97.16	98.03
CoroNet [20]	97.28	96.68	96.75	97.63	97.55	98.42
CovidXrayNet [24]	96.66	96.11	96.13	97.06	96.98	97.85
DarkCovidNet [31]	94.04	93.46	93.51	94.41	94.33	95.2
Proposed QCML model	98.69	98.11	98.16	99.06	98.98	99.85
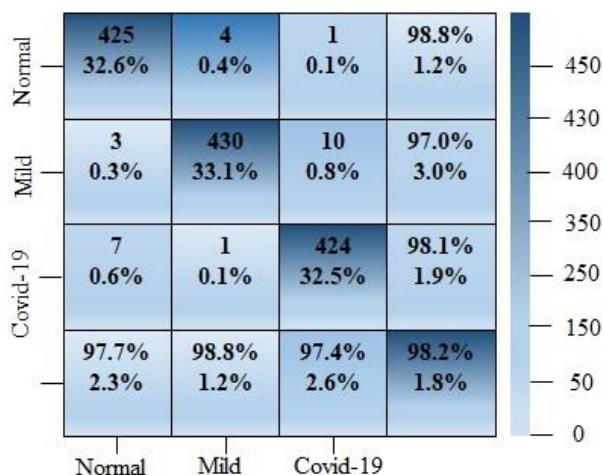
FIGURE 8. Confusion Matrix

The results of an experimental investigation employing the dataset I, which comprises of CT scans utilised for identifying Covid-19, are shown in TABLE 2. This table contains the information. The model earned the greatest performance overall across all measures, resulting in a success rate of one hundred percent. The confusion matrix of the proposed system is shown in FIGURE 8. In the second application, experimental research was carried out by integrating the dataset I and dataset II, both of which comprise CT scans of Covid-19 and normal instances. This was done so that the results of the study could be used to the second application. The findings are shown in TABLE 3, where it is possible to see that the proposed method QCML was successful in reaching the greatest possible success rate of 95.52% according to the accuracy metric.

TABLE 3
Performance comparison with dataset II

Model	Accuracy (%)	Precision	Recall	F1-Score	Specificity (%)	AUC (%)
DenseNet	87.77	87.11	85.52	87.28	87.74	87.58
AlexNet	82.19	81.53	79.94	81.7	82.16	82
ResNet	83.12	82.46	80.87	82.63	83.09	82.93
CspNet [21]	81.26	80.6	79.01	80.77	81.23	81.07
VGG16	46.07	45.41	43.82	45.58	46.04	45.88
VGG19	46.07	45.41	43.82	45.58	46.04	45.88
CovXNet [22]	84.67	84.01	82.42	84.18	84.64	84.48
CoroNet [20]	87.93	87.27	85.68	87.44	87.9	87.74
CovidXrayNet [24]	86.84	86.18	84.59	86.35	86.81	86.65
DarkCovidNet [31]	84.6	83.94	82.35	84.11	84.57	84.41
Proposed QCML model	95.52	94.86	93.27	95.03	95.49	95.33

V. DISCUSSION

The Dataset-X-ray dataset was employed in the third experimental investigation that was conducted on identifying Covid-19. This dataset is comprised of four classes. The findings of the research are shown in TABLE 4. The proposed method QCML had the maximum performance in terms of accuracy (96.69%), precision (0.99), recall (0.98), F1-score (0.98).

TABLE 4
Performance comparison with dataset III

Model	Acc. (%)	Prec.	Recall	F1-Score	Spec. (%)	AUC (%)
DenseNet	86.98	0.89	0.9	0.89	88.68	93.14
AlexNet	90.5	0.92	0.92	0.92	89.14	94.74
ResNet	92.58	0.95	0.94	0.95	91.81	96.16
CspNet [21]	82.51	0.8	0.85	0.82	81.11	89.86
VGG16	90.97	0.93	0.92	0.93	88.61	94.9
VGG19	91.21	0.94	0.93	0.93	88.57	94.98
CovXNet [22]	92.32	0.96	0.9	0.92	90.3	93.78
CoroNet [20]	91.99	0.94	0.93	0.93	91.54	95.42
CovidXrayNet [24]	95.27	0.97	0.97	0.97	95.35	97.9
DarkCovidNet [31]	94.21	0.97	0.95	0.96	93.19	96.69
Proposed QCML model	96.69	0.99	0.98	0.98	96.56	99

Journal of Electronics, Electromedical Engineering, and Medical Informatics
Multidisciplinary: Rapid Review: Open Access Journal

Vol. 6, No. 2, April 2024, pp: 195-205; eISSN: 2656-8632

When it comes to classification and recognition tasks, convolutional neural networks, often known as CNNs, are frequently used. These networks make use of layers that are completely linked and are made up of feature maps that are produced using the convolution technique. These feature maps, which assist identify the characteristics recognised or preserved within the input, are produced by applying the filters that are employed in this procedure to the input picture. This produces the feature maps. Although while the feature maps that are closest to the output tend to capture more broad information, the network was built to recognise even the smallest of details in the picture that is being fed into it. The initial two layers of the convolution process each highlight a particular aspect of the pictures, which ultimately results in visuals that may be understood. These important traits are referred to as attributes, and although humans may have difficulty comprehending them, CNN models are able to understand them. Also, when feature maps progress deeper into the network, they have a tendency to expose less and fewer details, despite the fact that these details are relevant characteristics that are used in the decision-making process by CNN models. The heat maps of proposed model is shown in FIGURE 9.

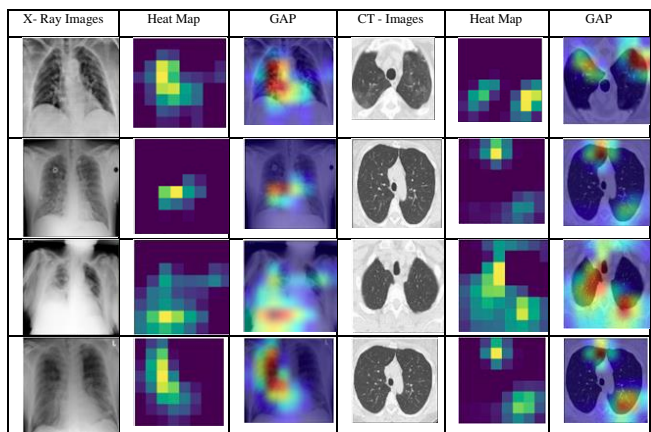When the findings of experimental research are considered as a whole, it can be observed that it makes accurate predictions of X-ray and CT pictures. As comparison to X-ray pictures, computed tomography (CT) images proved to be more successful. One possible explanation for this is that CT scans have a higher level of sensitivity and a more refined level of detail. FIGURE 10, FIGURE 11, and FIGURE 12 represents the performance comparison of all three datasets.

FIGURE 11. Performance comparison of proposed model using dataset II.

FIGURE 9. Sample heat maps and Covid-19 visuals of proposed model
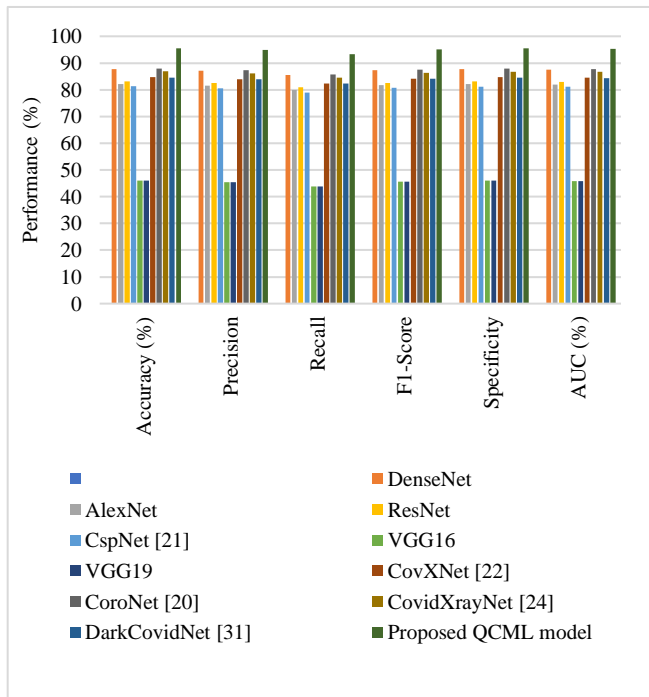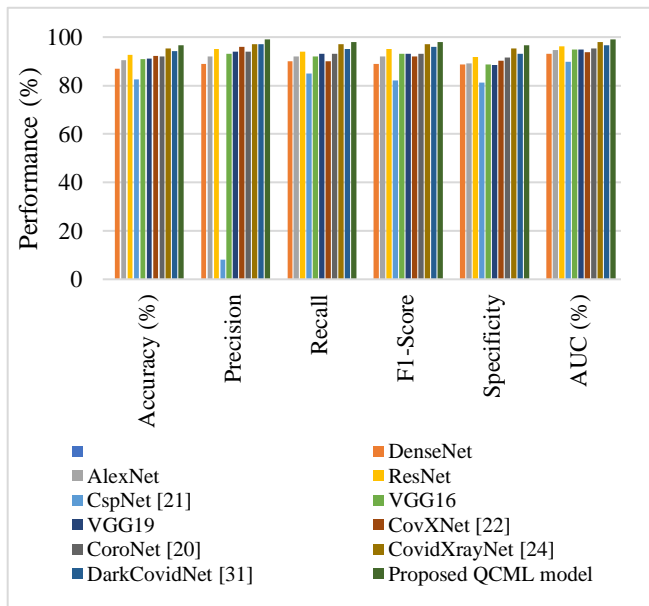

FIGURE 12. Performance comparison of proposed model using dataset III.

FIGURE 10. Performance comparison of proposed model using dataset I.

VI. CONCLUSION

The study aims to address the urgent need for accurate and efficient diagnostic methods for COVID-19, given the rising

number of cases and associated deaths. To this day, it has been responsible for the illness of millions of people and the death of millions more. The appearance of new strains of this disease presents significant dangers to human health, since the illness is known to be associated with a variety of adverse health effects. A number of states have taken a variety of preventative actions to stop the spread of the illness and cut down on the number of fatalities. In most cases, RT-PCR assays are used in order to make a diagnosis of this condition. Yet, there are a number of drawbacks associated with it, including the insufficiency of RT-PCR assays, the danger of transmission to healthcare professionals, the discomfort experienced by patients, and the expense. In this context, a variety of research projects are carried out, and a variety of potential solutions are proposed. One of these research looks at deep learning architectures that have a high level of performance. With an accuracy of 99.85%, a recall of 91.59%, a precision of 96.92%, and an F1-score of 94.18%, our suggested system demonstrated its better performance in comparison to other current systems. In future, it could be developed as an epidemiological models that can predict disease spread, identify high-risk populations, and inform public health interventions to control outbreaks effectively.

CONFLICTS OF INTEREST

The authors and co-authors declare that they have no conflicts of interest.

RESEARCH INVOLVING HUMAN PARTICIPANTS AND/OR ANIMALS

This article does not contain any studies involving animals performed and any studies involving human participants performed by any of the authors.

FUNDING INFORMATION

No funding for this research article.

INFORMED CONSENT

There is no human or animal sample was involved in this study.

REFERENCES

[1] F. Wu, et al., A new coronavirus associated with human respiratory disease in China, Nature 579 (7798) (2020) 265–269, http://dx.doi.org/10.1038/s41586-020-2008-3.

[2] Coronavirus disease (COVID-19) pandemic. https://www.who.int/emergencies/diseases/novel-coronavirus-2019.

[3] N. Subramanian, O. Elharrouss, S. Al-Maadeed, M. Chowdhury, A review of deep learning-based detection methods for COVID-19, Comput. Biol. Med.143 (2022) 105233, http://dx.doi.org/10.1016/j.compbiomed.2022.105233.

[4] G.D. Rubin, et al., The role of chest imaging in patient management during the COVID-19 pandemic, Chest 158 (1) (2020) 106–116, http://dx.doi.org/10.1016/j.chest.2020.04.003.

[5] R. Singh, et al., Corona virus (COVID-19) symptoms prevention and treatment: A short review, J. Drug Deliv. Ther. 11 (2-S) (2021) 118–120, http://dx.doi.org/10.22270/jddt.v11i2-S.4644.

[6] S. R, et al., An efficient hardware architecture based on an ensemble of deep learning models for COVID -19 prediction, Sustain. Cities Soc. (2022) 103713, http://dx.doi.org/10.1016/j.scs.2022.103713.

[7] A. Heidari, N. Jafari Navimipour, M. Unal, S. Toumaj, The COVID-19 epidemic analysis and diagnosis using deep learning: A systematic literature review and future directions, Comput. Biol. Med. 141 (2021) (2022) 105141, http://dx.doi.org/10.1016/j.compbiomed.2021.105141.

[8] J.M. Sharfstein, S.J. Becker, M.M. Mello, Diagnostic testing for the novel coronavirus, JAMA 323 (15) (2020) 1437, http://dx.doi.org/10.1001/jama.2020.3864.

[9] S. Stephanie, et al., Determinants of chest radiography sensitivity for COVID-19: A multi-institutional study in the United States, Radiol. Cardiothorac. Imaging 2 (5) (2020) e200337, http://dx.doi.org/10.1148/ryct. 2020200337.

[10] R. Liu, et al., Clinica Chimica Acta positive rate of RT-PCR detection of SARS-CoV-2 infection in 4880 cases from one hospital in Wuhan, China, from Jan to 2020, Clin. Chim. Acta 505 (March) (2020) 172–175, http://dx.doi.org/10.1016/j.cca.2020.03.009.

[11] M. Dramé, et al., Should RT-PCR be considered a gold standard in the diagnosis of COVID-19? J. Med. Virol. 92 (11) (2020) 2312–2313, http://dx.doi.org/10.1002/jmv.25996.

[12] J. Xie, et al., Characteristics of patients with coronavirus disease (COVID-19) confirmed using an IgM-IgG antibody test, J. Med. Virol. 92 (10) (2020) 2004–2010, http://dx.doi.org/10.1002/jmv.25930.

[13] H. Hassan, et al., Supervised and weakly supervised deep learning models for COVID-19 CT diagnosis: A systematic review, Comput. Methods Programs Biomed. 218 (2022) 106731, http://dx.doi.org/10.1016/j.cmpb. 2022.106731.

[14] P. Gaur, V. Malaviya, A. Gupta, G. Bhatia, R.B. Pachori, D. Sharma, COVID-19 disease identification from chest CT images using empirical wavelet transformation and transfer learning, Biomed. Signal Process. Control 71 (PA) (2022) 103076, http://dx.doi.org/10.1016/j.bspc.2021.103076.

[15] [14] Suganyadevi, S., Seethalakshmi, V. Deep recurrent learning based qualified sequence segment analytical model (QS2AM) for infectious disease detection using CT images. Evolving Systems (2023). https://doi.org/10.1007/s12530-023-09554-5

[16] F. Ucar, D. Korkmaz, COVIDiagnosis-Net: Deep Bayes-SqueezeNet based diagnosis of the coronavirus disease, 2019 (COVID-19) from X-ray images, Med. Hypotheses 140 (April) (2020) 109761, http://dx.doi.org/10.1016/j. mehy.2020.109761.

[17] E. Başaran, Classification of white blood cells with SVM by selecting SqueezeNet and LIME properties by mRMR method, Signal, Image Video Process (2022) http://dx.doi.org/10.1007/s11760-022-02141-2.

[18] G. Çelik, M.F. Talu, A new 3D MRI segmentation method based on generative adversarial network and atrous convolution, Biomed. Signal Process. Control 71 (PA) (2022) 103155, http://dx.doi.org/10.1016/j.bspc. 2021.103155.

[19] Suganyadevi, S., Seethalakshmi, V. & Balasamy, K. A review on deep learning in medical image analysis. Int J Multimed Info Retr (2021). https://doi.org/10.1007/s13735-021-00218-1

[20] I. Goodfellow, et al., Generative adversarial networks, Commun. ACM 63 (11) (2020) 139–144, http://dx.doi.org/10.1145/3422622.

[21] G. Çelik, M.F. Talu, Generating the image viewed from EEG signals, Pamukkale Univ. J. Eng. Sci. 27 (2) (2021) 129–138, http://dx.doi.org/10.5505/pajes.2020.76399.

[22] A. Esteva, et al., Dermatologist-level classification of skin cancer with deep neural networks, Nature 542 (7639) (2017) 115–118, http://dx.doi.org/10.1038/nature21056.

[23] J.H. Tan, et al., Automated segmentation of exudates, haemorrhages, microaneurysms using single convolutional neural network, Inf. Sci. (Ny) 420 (2017) 66–76, http://dx.doi.org/10.1016/j.ins.2017.08.050.

[24] E. Başaran, Z. Cömert, Y. Çelik, Neighbourhood component analysis and deep feature-based diagnosis model for middle ear otoscope images, Neural Comput. Appl. (2022) http://dx.doi.org/10.1007/s00521-021-06810-0.

[25] Y. Celik, M. Talo, O. Yildirim, M. Karabatak, U.R. Acharya, Automated invasive ductal carcinoma detection based using deep transfer learning with whole-slide images, Pattern Recognit. Lett. 133 (2020) 232–239, http://dx.doi.org/10.1016/j.patrec.2020.03.011.

[26] Bozdag, F.M. Talu, Pyramidal nonlocal network for histopathological image of breast lymph node segmentation, Int. J. Comput. Intell. Syst. 14 (1) (2021) 122–131, http://dx.doi.org/10.2991/ijcis.d.201030.001.

[27] M. Talo, O. Yildirim, U.B. Baloglu, G. Aydin, U.R. Acharya, Convolutional neural networks for multi-class brain disease detection using MRI images, Comput. Med. Imaging Graph. 78 (2019) 101673, http://dx.doi.org/10.1016/j.compmedimag.2019.101673.

[28] Suganyadevi, S., Seethalakshmi, V. CVD-HNet: Classifying Pneumonia and COVID-19 in Chest X-ray Images Using Deep Network. Wireless Pers Commun (2022). https://doi.org/10.1007/s11277-022-09864-y

[29] G. Gaál, B. Maga, A. Lukács, Attention U-net based adversarial architectures for chest X-ray lung segmentation, CEUR Workshop Proc. 2692 (2020) 1–7.

[30] J.C. Souza, J.O. Bandeira Diniz, J.L. Ferreira, G.L. França da Silva, A. Corrêa Silva, A.C. de Paiva, An automatic method for lung segmentation and reconstruction in chest X-ray using deep neural networks, Comput. Methods Programs Biomed. 177 (2019) 285–296, http://dx.doi.org/10.1016/j.cmpb.2019.06.005.

[31] Ö. Yıldırım, P. Pławiak, R.S. Tan, U.R. Acharya, Arrhythmia detection using deep convolutional neural network with long duration ECG signals, Comput. Biol. Med. 102 (September) (2018), 411–420, http://dx.doi.org/10.1016/j.compbiomed.2018.09.009.

AUTHOR BIOGRAPHY

G.Naga Chandrika is an Assistant Professor in the department of IT at VNR Vignana Jyothi Institute of Engineering and Technology, Hyderabad, Telangana, India. She received B.Tech degree in Computer Science and Information Technology from JNTU, Hyderabad, India in 2002 M.Tech in Software Engineering from JNTU, Anantapur in 2004 and Ph.D in Computer Science and Engineering from ANU, Guntur in 2022. She has published around 20 papers in international journals and conferences. She is serving as a reviewer for reputed journals like Computers, Materials and Continua, Computer Systems Science and Engineering. Her areas of interest include Social Network Analysis, Machine Learning, Medical Imaging, and Image Processing.
Email: nchandrika_g@vnrvjiet.in

J. Karpagam, completed Master's degree in the specialization of Power Electronics and Drives and doctoral degree in Electrical Engineering from Anna University Chennai, India. Presently she is working as Professor in the department of Electrical and Electronics Engineering at Karpagam University, Coimbatore, India and she is in this profession since 1999. Her area of interest includes Power Electronics, DSP applications to Power Electronics and Wind Energy Conversion System, Solid State Drives, Power Converters. So far, she has published around 45 research articles in national, international conferences and journals. She has received funding of around 15 Lakhs from various organizations such as AICTE, ICMR etc. She has been acted as resource person for the technical session and reviewer for journals. Dr. Author was a recipient of the International Association of Geomagnetism and Aeronomy Young Scientist Award for Excellence in 2008, and the IEEE Electromagnetic Compatibility Society Best Symposium Paper Award in 2011.
Email: jkarpagam123@gmail.com

Mr. Titus Richard is currently a faculty in the department of Biosciences and a facilitator of English Language with ample experience in English language teaching and training. He received his undergraduate and postgraduate degrees in English from the Madurai Kamaraj University, Madurai. Currently he is pursuing her PhD from Saveetha University, Chennai, India. He has a diversified research record of publishing like in Scopus that includes 6 papers and 1 design patent. His likely research areas include English Language Teaching, CALL, MALL, AI Integrated Teaching Aids, Virtual Reality, Materials etc. He is also a life time member of English Language Teachers' Association of India (ELTAI) and English Language Teachers' Interaction Forum (ELTIF).
Email: titusrichad@gmail.com

Dr. Finney Daniel Shadrach holds a Bachelor's degree in Electronics and Communication Engineering, a Master's degree in Communication Systems, and a Ph.D. degree. from Anna University. Currently, he is serving as an Assistant Professor at KPR Institute of Engineering and Technology in Coimbatore, India. His research interests include signal processing, image processing, optimization techniques, and deep learning. He has published more than 30+ research articles in reputed international conferences and journals. He is an active reviewer for esteemed journals such as Springer, Sage, etc,. He is a lifetime member of ISTE and a member of IEEE.
Email: finneydaniels@gmail.com

Dr. T. Triwiyanto received the B.S. degree in Physics from Airlangga University, Indonesia, M.S. degree in Electronic Engineering from the Institut Teknologi Sepuluh Nopember Surabaya, Indonesia, in 2004, and a Ph.D. degree in Electrical Engineering from Gadjah Mada University, Yogyakarta, Indonesia, in 2018. From 1998 to 2004, he was a Senior Lecturer with the Microcontrollers Laboratory. Since 2005, he has been an Associate Professor with the Medical Electronics Technology Department, Health Polytechnic Ministry of Health Surabaya, Indonesia. In 2018, Triwiyanto received the best Doctoral Student award from Gadjah Mada University. Additionally, he is Editor-in-chief in several peer review journals and chairman Technical Programme Committee at several International Conferences. His current research interests include a microcontroller, electronics, biomedical signal processing, machine learning, rehabilitation engineering, and surface electromyography (sEMG)-based physical human-robot interactions. I have published over 80 papers in reputable journals and conferences. My Scopus h-index is 13, which reflects the impact of my research. I am a proud member of the IEEE (Institute of Electrical and Electronics Engineers). You can find my complete publication record and more details on my Scopus profile here. (email: triwiyanto@ieee.org)